Radiology

REVIEWS AND COMMENTARY • REVIEW

The Future Is Beyond Bright: The Evolving Role of Quantitative US for Fatty Liver Disease

Arinc Ozturk, MD • Viksit Kumar, PhD • Theodore T. Pierce, MD, MPH • Qian Li, MD • Masoud Baikpour, MD • Ivan Rosado-Mendez, PhD • Michael Wang, PhD • Peng Guo, PhD • Scott Schoen Jr, PhD • Yuyang Gu, PhD • Sunethra Dayavansha, PhD • Joseph R. Grajo, MD • Anthony E. Samir, MD, MPH

From the Center for Ultrasound Research & Translation, Department of Radiology, Massachusetts General Hospital, 101 Merrimac St, 3rd Floor, 323G, Boston, MA 02114 (A.O., V.K., T.T.P., Q.L., M.B., P.G., S.S., Y.G., S.D., A.E.S.); Harvard Medical School, Boston, Mass (A.O., V.K., T.T.P, Q.L., A.E.S.); Departments of Medical Physics and Radiology, University of Wisconsin, Madison, Wis (I.R.M.); GE HealthCare, Milwaukee, Wis (M.W.); and Department of Radiology, University of Florida, Gainesville, Fla (J.R.G.). Received December 12, 2022; revision requested December 30; revision received April 18, 2023; accepted May 8. **Address correspondence to** A.O. (email: *aozturk@mgh.harvard.edu*).

T.T.P. was supported by the 2020 American Roentgen Ray Society Scholar Award. A.E.S. was supported by the National Institute of Diabetes and Digestive and Kidney Diseases of the National Institutes of Health under award no. R01 DK119860. Any opinions, findings, conclusions, or recommendations expressed in this material are those of the author(s) and do not necessarily reflect the views of the National Institutes of Health.

Conflicts of interest are listed at the end of this article.

Radiology 2023; 309(2):e233146 • https://doi.org/10.1148/radiol.223146 • Content codes: GI US

Nonalcoholic fatty liver disease (NAFLD) is a common cause of morbidity and mortality. Nonfocal liver biopsy is the historical reference standard for evaluating NAFLD, but it is limited by invasiveness, high cost, and sampling error. Imaging methods are ideally situated to provide quantifiable results and rule out other anatomic diseases of the liver. MRI and US have shown great promise for the noninvasive evaluation of NAFLD. US is particularly well suited to address the population-level problem of NAFLD because it is lower-cost, more available, and more tolerable to a broader range of patients than MRI. Noninvasive US methods to evaluate liver fibrosis are widely available, and US-based tools to evaluate steatosis and inflammation are gaining traction. US techniques including shear-wave elastography, Doppler spectral imaging, attenuation coefficient, hepatorenal index, speed of sound, and backscatter-based estimation have regulatory clearance and are in clinical use. New methods based on channel and radiofrequency data analysis approaches have shown promise but are mostly experimental. This review discusses the advantages and limitations of clinically available and experimental approaches to sonographic liver tissue characterization for NAFLD diagnosis as well as future applications and strategies to overcome current limitations.

Chronic liver disease (CLD) affects 1.5 billion people worldwide (1). CLD can be caused by metabolic, environmental, infectious, or genetic factors. Across causes, CLD progresses through repeated cycles of liver injury and fibrosis in which ongoing inflammation and hepatocellular injury result in progressive scarring that can ultimately culminate in cirrhosis.

Nonalcoholic fatty liver disease (NAFLD), or metabolic dysfunction–associated steatotic liver disease (MASLD) in new terminology, is the most common CLD cause and is characterized by fat accumulation in vacuoles within the hepatocytes without alcohol-related liver injury (2). Nonalcoholic steatohepatitis (NASH), or metabolic dysfunction–associated steatohepatitis (MASH) in new terminology, is a subtype of NAFLD in which inflammation and hepatocellular injury result in fibrosis and, ultimately, advanced CLD. Some patients with NASH accompanied by severe fibrosis (grade ≥F2) and inflammation (NAFLD activity score ≥4) at first diagnosis have an elevated long-term risk of cirrhosis (3,4), termed high-risk NASH (3,4). Currently, there are no treatment options cleared by the U.S. Food and Drug Administration (FDA) for patients with high-risk NASH, but a variety of therapeutics are in development. It is important to identify patients with NAFLD, as they are at risk for the development of NASH. Early NASH and particularly high-risk NASH diagnosis and treatment may provide an opportunity to prevent cirrhosis-related complications, such as portal hypertension, hepatic encephalopathy, and hepatocellular carcinoma. Estimation of inflammation and fibrosis in patients with NAFLD provides prognostic information and helps identify patients with high-risk disease. However, ultimately, a tool for identifying patients with NAFLD at risk for progression would be ideal to aid in early detection. Recent pilot data suggest that imaging estimates of steatosis severity may help identify patients at risk for progressive disease (5).

Liver biopsy is the accepted reference standard tool for NAFLD risk stratification but is limited by invasiveness and high cost. MRI-based methods such as proton density fat fraction (PDFF) estimation and MR elastography are accurate methods to quantify steatosis and fibrosis, respectively (6), but their use is constrained by relatively high cost and limited availability. US-based methods have favorable cost and wide availability, making them more suitable for population-level diagnosis and risk stratification.

This review focuses on currently available US methods to evaluate liver steatosis, inflammation, and fibrosis. Each section summarizes different US-based methods, current evidence, and future directions. We also discuss recent promising innovations that are not yet clinically available. Our goal is to discuss these technologies and place them into a broader context for the practicing radiologist. For more detailed technical discussion, we refer the reader to the recent article by Fetzer and Rosado-Mendez et al (7).

Abbreviations

AC = attenuation coefficient, AI = artificial intelligence, ASQ = acoustic structure quantification, AUC = area under the receiver operating characteristic curve, CLD = chronic liver disease, FDA = U.S. Food and Drug Administration, HRI = hepatorenal index, NAFLD = nonalcoholic fatty liver disease, NASH = nonalcoholic steatohepatitis, NLV = normalized local variance, PDFF = proton density fat fraction, SoS = speed of sound, SWD = shear-wave dispersion, SWE = shear-wave elastography, SWV = shear-wave viscosity

Summary

Quantitative US techniques are noninvasive methods to quantify fatty liver disease severity; innovations in acoustics and image analysis disciplines show promising results in fatty liver diagnosis and risk stratification.

Essentials

- Noninvasive, low-cost, and accurate imaging-based quantification tools are needed to address the increasing incidence of fatty liver disease.
- Several tools are currently available, with varying evidence to support their role in detecting and assessing nonalcoholic fatty liver disease (NAFLD); these include shear-wave elastography and estimation of parameters such as attenuation coefficient, sound speed, hepatorenal index, and pulsatility index.
- Multiple advanced signal processing and image analysis methods for NAFLD and nonalcoholic steatohepatitis evaluation will likely be clinically available in the next 3–5 years.

Imaging Methods in Current Clinical Use for Liver Steatosis

Conventional US

Qualitative assessment of conventional gray-scale brightness mode (B-mode) US imaging has traditionally been the cornerstone of hepatic steatosis evaluation. Liver sonography is often performed as the first-line test to investigate abnormal liver function, and the diagnosis of steatosis may be the explanatory factor. Characteristic findings of fat deposition include increased parenchymal echogenicity, beam attenuation, blurring of anatomic structures (such as the intrahepatic vasculature, gallbladder wall, or diaphragm), and image quality degradation (Fig 1). Generally, echogenicity assessment is performed by comparing the liver tissue with the other hepatic structures (eg, vessel walls) or adjacent organs (eg, kidney). The characteristic B-mode findings result from a combination of aberrations due to assumed and actual parenchymal sound speed mismatch, increased backscattered echoes from lipid droplets, and increased beam attenuation due to increased backscatter and absorption. Hepatic fat deposition is often heterogeneous, with characteristic areas adjacent to the gallbladder fossa, falciform ligament, or portal vein that remain uninvolved, possibly due to variability in venous drainage and perfusion in these regions (8). Moderate to severe steatosis can be detected with 84.8% sensitivity (95% CI: 79.5, 88.9) and 93.6% specificity (95% CI: 87.2, 97) at B-mode US, as published in a meta-analysis (9). However, sensitivity and specificity for mild steatosis could be lower (70% [95% CI: 63, 77] and 86% [95% CI: 82, 89], respectively), as published in another meta-analysis (10).

B-mode features of steatosis are subjective, with corresponding interpretative variability and limited generalizability. Furthermore, technical acquisition parameters can confound some features. Increasing overall image gain or changing US transducer frequency can lead to increased parenchymal echogenicity, while altering depth-dependent time gain compensation settings can mimic increased beam attenuation. Generalized image quality reduction may result from several factors, including acquisition hardware differences, transducer transmit frequency, sonographer technical skill, and increased patient abdominal subcutaneous tissue thickness. Variation in interpreting radiologist experience may confound reader reliability. These pitfalls commonly make interpretation challenging, even for experienced readers. Identifying fatty sparing in characteristic locations can improve interpretation specificity, as technical parameters may have less influence on this feature. Nonetheless, the limitations of conventional B-mode US for liver steatosis estimation are well established.

The hepatorenal index (HRI) is a semiquantitative B-mode imaging steatosis biomarker derived by dividing the hepatic B-mode signal intensity by the renal cortical signal intensity at the same depth (to account for attenuation effects) (11) within a single image depicting both structures (Fig 2). This aims to mitigate confounding parameters by standardizing liver brightness estimation to the renal cortex as an internal control. Higher HRI values indicate increased liver echogenicity and correspond to increased steatosis. Some vendors offer an HRI calculation tool in their US device commercial software, with a subset allowing HRI estimation from the acquired raw data to mitigate confounding from time gain compensation settings. However, the HRI measurement may still be confounded by concomitant renal disease, which alters the brightness of the kidney parenchyma.

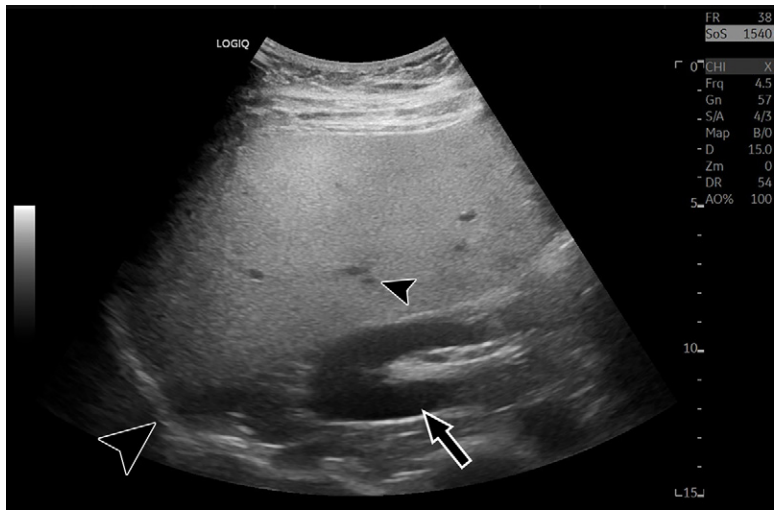

Figure 1: Characteristic B-mode US image in a 35-year-old male patient with hepatic steatosis and 16% MRI proton density fat fraction. Steatosis results in increased brightness of the liver relative to the kidney (arrow), blurring of hepatic vasculature (small arrowhead), loss of definition of the diaphragm (large arrowhead), and reduced signal from deep anatomy.

Figure 2: B-mode US image at the level of the pouch of Morison in a 59-year-old female patient with nonalcoholic steatohepatitis and grade 2 hepatic steatosis. Two circular regions of interest are placed on the kidney cortex and liver tissue at the same depth. Hepatorenal index (HRI) can be calculated on US systems with HRI quantification software, or images can be exported in Digital Imaging and Communications in Medicine, or DICOM, format and region of interest circles can be drawn with a DICOM viewer. In this image, the local region of interest pixel brightness values and the HRI value are presented in the bottom left corner. Reproduced, with permission, from the Non-Invasive Biomarkers of Metabolic Liver Disease, or NIMBLE 1.1, study (18).

Additionally, changing device acquisition settings may influence the appearance of the images available for postacquisition HRI measurement, implying that standardized settings may be needed for reliable HRI measurements. The reported sensitivity (76.4% [95% CI: 70.2, 82.7]) and specificity (93.2% [95% CI: 86.4, 98.3]) of HRI with a cutoff value of 1.22 to detect steatosis in a prospective multicenter study with biopsy-proven CLD cases including NAFLD suggest that it may have clinical value (12,13). However, the technique is limited by the fact that liver fibrosis, which is a parameter of interest, may confound the relationship between HRI and hepatic steatosis (14).

In summary, although B-mode–based methods are common and easy to access, they have several disadvantages, as described earlier. To address these limitations, methods such as deep learning may decrease manual region of interest drawing workload and provide accurate HRI estimation (15). Artificial intelligence (AI)–enhanced screening of B-mode images to identify patients with suspected steatosis may be helpful to refer patients to more advanced methods, such as PDFF, or more accurate US-based methods, such as attenuation coefficient (AC) estimation.

Attenuation Coefficient

US AC is defined as the measure of the rate of energy lost by the acoustic wave as it propagates through the tissue, quantified in decibels per unit of depth (in centimeters). Attenuation is dependent on insonation frequency and tissue characteristics, so it is normalized by the frequency (relative to 1 MHz). Thus, the AC has a unit of dB/cm/MHz. Attenuation can be quantified by accounting for the energy lost in the propagating tissue at different frequencies. Different factors affect attenuation estimation accuracy, including focus depth, varying backscatter and speed of sound (SoS), imaging resolution, artifacts, and signal-to-noise ratio of the echo. US AC estimation is available on multiple FDA-cleared US devices. Further details describing AC estimation can be found in a review article by Ferraioli et al (16).

AC for fatty liver evaluation has been studied more than other quantitative US fat quantification methods. It is known that higher attenuation values are present in liver tissues with higher steatosis severity. Many studies have been published regarding the diagnostic accuracy, variability, and operator dependence of these methods (16,17). In a recent meta-analysis of 13 studies, the pooled sensitivity and specificity for attenuation-related methods to diagnose steatosis severity were 76% (95% CI: 73, 80; I^2 = 43% [I^2 is a marker of heterogeneity]) and 84% (95% CI: 77, 89; I^2 = 74%), respectively, for mild steatosis (≥S1) and 87% (95% CI: 83, 91; I^2 = 0%) and 79% (95% CI: 75, 83; I^2 = 59%) for moderate steatosis (≥S2) (17). These results suggest that AC may be a useful tool to diagnose and quantify steatosis severity.

Regarding operator dependence, high intra- and interobserver agreement values (intraclass correlation coefficient between 0.79 and 0.98) have been reported for attenuation imaging (16). However, it is important to consider the effects of operator training, experience, and device familiarity, as these factors may increase operator dependence. As attenuation imaging is available on multiple devices, interplatform agreement is another important factor that should be evaluated and is the subject of several active studies (18).

There is currently no widely accepted US AC measurement practice guideline. Some centers use elastography practice guidelines to perform US attenuation examinations, which include the following suggestions: *(a)* Liver attenuation measurements are typically taken with the patient in the supine or left lateral decubitus position at mid breath hold and *(b)* the region of interest should be placed on a homogeneous region more than 2 cm deep to the liver capsule to avoid capsule artifacts while avoiding blood vessels (Fig 3). Most vendors suggest taking five independent measurements of attenuation and reporting the median value; however, there is no strict recommendation or guideline regarding the required number of measurements. The utility of reporting the IQR divided by the median value, as is done for shear-wave elastography (SWE), is presently unclear (16). In summary, initial data regarding the diagnostic performance and variability of AC estimation for steatosis quantification are promising, but several unmet needs remain, including *(a)* widely accepted implementation guidelines, *(b)* understanding of measurement variability across manufacturers, and *(c)* understanding of how new AI technologies may be used in conjunction with the technique (19).

Other Commonly Used Methods

Changes in the number and size of intracellular fat vacuoles in steatosis result in a change of parenchymal echogenicity, producing a hyperechoic appearance compared with normal tissue or kidney. Techniques to discern these properties from the level of the acoustic echoes—termed the *backscatter coefficient*—have demonstrated similar performance to MRI-derived estimates of steatosis quantification (20–22). It is known that backscatter

coefficient values increase with increased steatosis level. However, more clinical studies are needed to understand operator dependence and other patient- and device-related confounding factors. Backscatter coefficient can be calculated from radiofrequency signal data (23).

SoS is another acoustic parameter that can be used to assess steatosis. SoS quantification provides reasonable delineation of disease severity, with known negative correlation between steatosis severity and SoS (Fig 4). Currently, the availability of this method on clinical devices is limited, as is the literature on the performance of SoS in clinical studies. However, recent studies show promising results to diagnose steatosis. In a cohort of 215 patients with NAFLD, SoS estimation showed an area under the receiver operating characteristic curve (AUC) of 0.88 (95% CI: 0.82, 0.92) to detect grade S2 or higher (24). A widely acceptable reference standard like biopsy or PDFF was not available in this recent study. More clinical studies are needed to understand the effect of confounding factors and device and operator variability on the SoS biomarker.

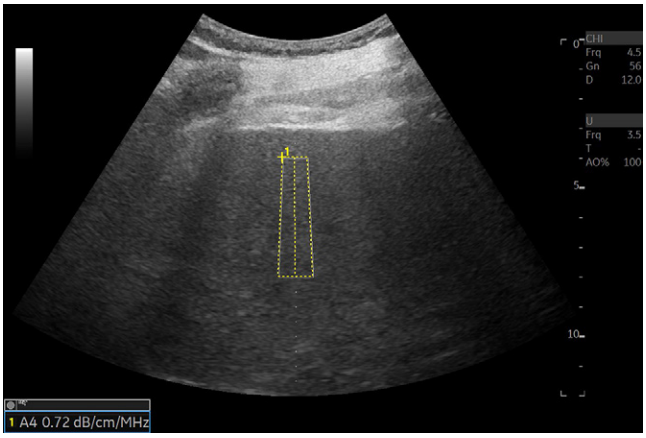

Figure 3: US image in a 72-year-old male patient with nonalcoholic steatohepatitis and grade 1 steatosis shows an example of US liver attenuation coefficient measurement. Higher attenuation values are expected with higher grades of steatosis. A region of interest is placed on an area without visible blood vessels. Attenuation value is presented on the bottom left of the image. Attenuation measurements are collected from the rectangular region of interest. Color map may be added to the region of interest if needed. Reproduced, with permission, from the Non-Invasive Biomarkers of Metabolic Liver Disease, or NIMBLE 1.1, study (18).

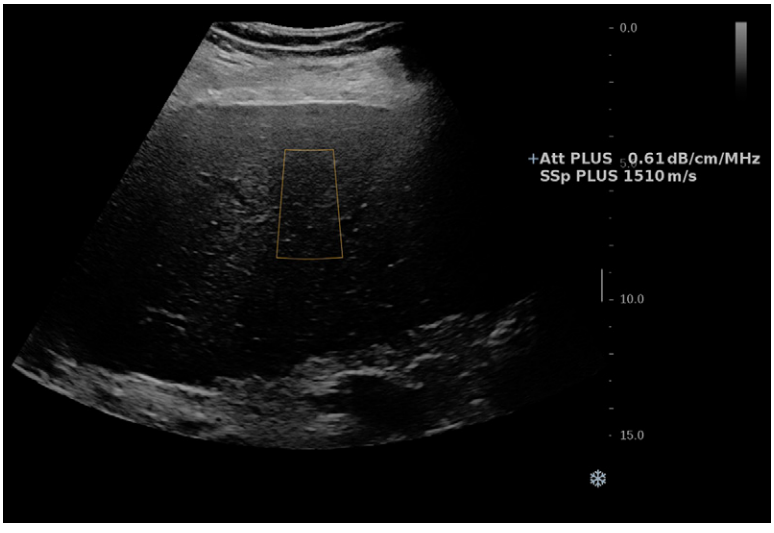

Figure 4: US image in a 64-year-old male patient with nonalcoholic steatohepatitis cirrhosis and grade 1 steatosis. Speed of sound (SSp PLUS) and attenuation (Att PLUS) values are shown. The measurements are collected from the rectangular region of interest. Lower speed of sound values are expected with increasing steatosis. Reproduced, with permission, from the Non-Invasive Biomarkers of Metabolic Liver Disease, or NIMBLE 1.1, study (18).

Other techniques combine measures (eg, attenuation and backscatter coefficient) to estimate a US-derived fat fraction (Fig 5) (22) and have demonstrated high performance in the diagnosis of steatosis when compared with the reference standard of MRI PDFF (AUC, 0.90 [95% CI: 0.79, 0.96] to detect greater than 5.5% PDFF value) (25) and also high reproducibility values (intraclass correlation coefficient higher than 0.93) (26). These results suggest that US-derived fat fraction may be an accurate and reproducible method to evaluate steatosis; however, studies with biopsy-proven (ideally single-pathologist) NAFLD may be needed to support the literature.

A persistent challenge for deriving material properties from US images is that these images depend both on individual machine settings (frequency, gain, focal depth, etc) and parameters that are set by the individual sonographer. Controls by way of a reference phantom or by comparison with the appearance of another target, such as the kidney cortex (ie, the HRI), have been proposed to mitigate interoperator and intersession variability. Modern implementations of these techniques rely on internal validation and correction strategies that are embedded in the device, which mitigates the need for external validation tools, such as phantoms.

Backscatter coefficient, SoS, and US-derived fat fraction show promising results in terms of steatosis quantification. US-derived fat fraction and SoS methods are available on clinical systems, but access to raw data may be needed to calculate backscatter coefficient. Cooperative efforts to standardize approaches across manufacturers and provide access to raw data under appropriate legal terms may be crucial to use these methods reliably in clinical settings.

Speckle Statistics

Speckle patterns appear in US images due to scattered US signals from tissue microstructures. Therefore, speckle statistics, representing the envelope distribution of backscattered US signal, are a good indicator of tissue scattering characteristics. Advanced quantitative US techniques based on these envelope parameters, such as acoustic structure quantification (ASQ), normalized local variance (NLV), and Nakagami distribution, have been developed as potential biomarkers for fat quantification. Most of these methods are commercially available; however, the literature is limited on the comparison of these with the other NAFLD assessment tools. We summarize these methods in the Table and Figure 6.

In the ASQ method, the degree of deviation from the Rayleigh distribution is quantified to assess the liver tissue characteristics (Fig 6). Theoretically, ASQ is used to compute a focal disturbance

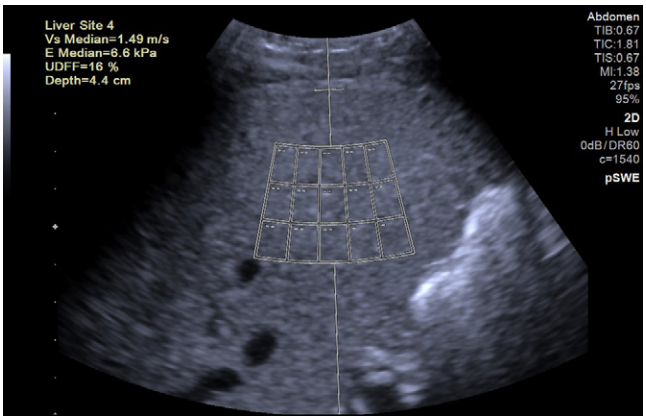

Figure 5: US image in a 55-year-old female patient with nonalcoholic steatohepatitis and grade 1 steatosis. Point shear-wave elastography (pSWE) and US-derived fat fraction (UDFF) measurements are presented. The device software uses a large region of interest with 15 small measurement locations (rectangles). In this method, attenuation and backscatter coefficients are combined to report a single value in percentage unit. Higher US-derived fat fraction values are expected with increasing steatosis. The US-derived fat fraction and shear-wave speed values (top left corner) are acquired by these 15 small regions of interest. The purpose of using 15 small regions of interest is to expand the measurement area. Reproduced, with permission, from the Non-Invasive Biomarkers of Metabolic Liver Disease, or NIMBLE 1.1, study (18).

ratio, which is inversely related to the fat content of the liver. In an early study, a significant negative correlation between the focal disturbance ratio and the MR spectroscopy–based hepatic fat fraction was demonstrated ($r = -0.87$; $P < .01$) (27). Similar negative correlation results have been shown in a recent study (28), and performance to diagnose MR spectroscopy–defined steatosis (≥5%) was also proven (AUC, 0.82) (29).

NLV is an extension of ASQ and provides a quantitative tool to perform regional analysis of the image and evaluate the intensity and homogeneity of the liver tissue. Lower NLV values have been associated with higher steatosis grade (30). The SD of NLV has been shown to help detect mild (AUC, 0.90 [95% CI: 0.74, 0.97]), moderate (AUC, 0.74 [95% CI: 0.56, 0.87]), and severe steatosis (AUC, 0.60 [95% CI: 0.42, 0.76]) (31). Generally, with the other steatosis quantification methods, higher AUCs may be observed in the detection of severe steatosis, but the opposite could be possible for NLV, considering the results from Zhao et al (31). In a separate study (32), NLV showed high repeatability with an intraclass correlation coefficient of 0.87 (95% CI: 0.61, 0.95) and reproducibility with intraclass correlation coefficient of 0.80 (95% CI: 0.50, 0.92) in assessing PDFF-proven steatosis. These studies show promising results, but sample sizes were small; meta-analyses may be needed to understand the cumulative effect.

Last, the Nakagami parameter, another modern technique, is the variation in the shape of the envelope distribution of backscattered US signal. Increased Nakagami parameter values have been associated with higher steatosis severity (33). In a recent study (33), the Nakagami parameter was indicative of mild steatosis (PDFF ≥6.4%), with an AUC of 1.00. Although high correlation with PDFF has been reported by some authors, others have not shown as promising results, with lower correlation ($r = 0.47$) with PDFF (34). Further studies with larger samples are needed to understand the diagnostic performance of this method.

Tissue scatter distribution imaging and tissue attenuation imaging, other commonly used techniques, provide attenuation and Nakagami parameter values. High diagnostic accuracy was observed when using this combination of methods, the details of which can be found in another review (35).

ASQ, NLV, and Nakagami parameters may be useful methods in the diagnosis of NAFLD. Although the diagnostic performance has been reported as high in recent studies, it is important to note that the literature regarding these parameters is limited, and reported results may not be generalizable. Additionally, the effect of several confounding factors like obesity, patient movement, and breath intake are not well established.

Shear-Wave Elastography, Dispersion, and Viscosity

In US SWE, tissue stiffness is estimated by inducing shear waves in tissue, most commonly with acoustic radiation force, and measuring the propagation velocity of those shear waves. Based on the measurement area size, it can be categorized as point SWE or two-dimensional SWE. Higher shear-wave velocities are associated with increased fibrosis severity or increased tissue stiffness (36). SWE estimates of tissue stiffness can be reported as the estimated Young modulus of tissue in kilopascals or as shear-wave speed in meters per second; conversion between these properties is algebraic. Multiple studies have shown that SWE can be used to distinguish cirrhosis from early-stage liver fibrosis with excellent accuracy and differentiate intermediate liver fibrosis stages with moderate accuracy (37). As a result, SWE-derived hepatic shear-wave speed estimates have been widely adopted as liver fibrosis biomarkers. SWE is in widespread clinical use but is limited by variability produced by operator-, patient-, and device-related factors (Fig 7). Details about common SWE limitations and artifacts can be found in the paper by Bruce et al (38).

Shear-wave dispersion (SWD) has been proposed as a biomarker for inflammation and has been studied in several clinical studies (39). Higher SWD values have been associated with higher grades of histopathologic ballooning and lobular inflammation (40). When combined with AC, SWD may show higher diagnostic performance in the detection of NASH, even higher than SWE alone. These results show that combining parameters, such as AC, SWE, and SWD, may improve diagnostic performance for identifying patients with high-risk NASH (41).

Last, shear-wave viscosity (SWV), another shear wave–focused biomarker, has been used in several clinical studies. No significant relationship has been shown between SWV and PDFF-based steatosis severity (34,42); however, SWV may be related to the degree of fibrosis (AUC, 0.76 [95% CI: 0.64, 0.87] for significant fibrosis), with higher viscosity values at higher fibrosis stages (43). No association was found between SWV and steatosis or disease activity (43). One of the strong sides of this study is that the biopsy samples were evaluated by one pathologist, which minimizes the reader variability on the reference standard side.

SWE, SWD, and SWV may be estimated during a single US examination. The diagnostic performance of SWE

Common Sonographic NAFLD Evaluation Methods

Method	Physics	Area of Use	Challenges	Recommended Articles for Details
Shear-wave elastography	Uses shear-wave velocity to identify the elastic properties of the tissue	Fibrosis quantification	Depth dependency creates a variability challenge (37,48); strict protocol compliance (ROI at 4–4.5-cm depth, perpendicular ROI in reference to the capsule) may be needed to acquire accurate stiffness measurements with low variability	37, 38, 62–64
Shear-wave dispersion	Shear wave–based analysis (m/sec/kHz unit)	Inflammation	Limited clinical data; possible confounding effect from fibrosis or steatosis	33, 34
Hepatorenal index	Semiquantitative assessment of backscatter due to steatosis, using renal cortex as an internal control	Steatosis quantification	Confounding from renal disease and liver fibrosis; proposed thresholds are highly variable; manual ROI placement	65
Attenuation coefficient	Quantifies energy loss in different tissue types	Steatosis quantification	Cause of liver disease, uneven fat distribution, liver inflammation, fibrosis, and body habitus; signal bandwidth, frequency, and phase aberration	17
Backscatter coefficient	Compares reflected acoustic energy with reference	Steatosis quantification, microstructure information	Calibration (eg, frequency-dependent); microstructure assumptions (eg, size distributions of scatterers alter measurements)	23
Speed of sound	Rate of longitudinal sound wave propagation in tissue	Steatosis quantification; beamforming and image quality improvement	Limited commercial availability and clinical data; estimation may be biased for layered media	66, 67
US-derived fat fraction	Compares attenuation and backscatter coefficient with reference phantom	Steatosis quantification	Possible effect of subcutaneous tissue; ROI placement may be affected by local structures like vessels	22, 25
ASQ	Difference in theoretical and real envelope distributions of backscattered US signal	Fibrosis and steatosis quantification	Limited clinical data; limited performance with large hepatic vessels, focal fat sparing or deposition, and artifacts	28, 29, 68
Normalized local variance	Modified ASQ for regional evaluation of intensity and homogeneity	Steatosis quantification	Limited clinical data; influence of ROI size; limitations in diagnosing severe steatosis; limited performance with large hepatic vessels, focal fat sparing or deposition, and artifacts	31, 69
Nakagami parameter	Variation in the shape of the envelope distribution of backscattered US signal	Fibrosis and steatosis quantification	Parameter plateaus for high scatter concentrations	34, 35, 70
Spectral Doppler US	Measures blood flow dynamics	Fibrosis quantification	Need stronger literature knowledge; selecting minimum and maximum velocity is operator-dependent	46
Mean scatter spacing analysis	Change of the periodicity of US signal	Inflammation and fibrosis	In vivo validation and real-time estimation	71

Table *(continues)*

for fibrosis staging is well known. More clinical studies are needed for SWD and SWV to better understand their association with inflammation and fibrosis and the magnitude of the effect of common confounders, including obesity, food intake, and patient movement.

Several future directions to improve and combine these biomarkers have been proposed. Researchers have proposed increasing the acoustic output to obtain higher-quality SWE images in difficult-to-image patients, especially in patients with obesity and increased subcutaneous tissue thickness (44). Multiple frequency–induced reverberant shear waves may be helpful to obtain higher-quality SWD data in patients with increased subcutaneous tissue thickness (45) and may specifically be helpful to detect inflammation. Combined fibrosis,

Table *(continued)*: Common Sonographic NAFLD Evaluation Methods

Method	Physics	Area of Use	Challenges	Recommended Articles for Details
Intensity spectrum	Several features related to microstructural organization of tissue (random vs organized, spacing between periodic scatterers) are extracted from the frequency-dependent (spectral) analysis of echo signals	Detection of changes in tissue microstructure due to diffuse liver disease	Sensitivity of features is obscured by other spectral components such as diffuse scattering, attenuation, and system effects	72
Spectral correlation and generalized spectrum	Detection of mean scatterer spacing, hypothesized to be associated with spacing among portal triads	Monitor microstructural remodeling due to diffuse or focal liver disease, and response to treatment	Consistency in scatterer spacing is needed to detect spectral correlation peaks related to periodic scatterers over diffuse component; scatterer spacing may depend on plane of insonation	73, 74
Analysis of phase uniformity	The presence of regularly paced scattering sources in the liver (ie, portal triads) produces a nonuniform distribution of the phase (stage of oscillation) of the arriving echo signal	Monitor microstructural remodeling due to diffuse or focal liver disease, and response to treatment	Consistency in scatterer spacing is needed to detect periodic scatterers over diffusely organized scatterers in the phase uniformity test; the degree of phase nonuniformity depends on the angle of insonation	75
H-scan	Extracts information about size and type of scattering agents by filtering the echo signals with gaussian-weighted Hermite functions	Monitor microstructural remodeling due to diffuse or focal liver disease	Depth-dependent effects, such as attenuation and diffraction	76, 77

Note.—ASQ = acoustic structure quantification, NAFLD = nonalcoholic fatty liver disease, ROI = region of interest.

steatosis, and inflammation assessment tools may help identify patients with NAFLD who are at risk of developing NASH and those with established high-risk NASH. For example, using SWE, SWD, and attenuation in the same US examination in the same region of interest would be cost- and time-efficient and provide full characterization to identify patients in need of aggressive treatment. Considering the high prevalence of NAFLD, the use of these combined tools for screening at the primary care level with point-of-care devices could provide a population-level solution to identify at-risk patients in need of specialized care.

Portal Venous and Other Waveform Analysis

Hepatic Doppler US is widely accepted as a valuable, noninvasive, and cost-effective tool that is considered a first-line imaging technique for evaluating the hepatic vasculature. A hepatic Doppler US examination consists of gray-scale or B-mode US, color Doppler US, and spectral waveform analysis obtained by placing a small region of interest over a vessel of interest.

Each of the main vessels assessed during a liver Doppler US examination have characteristic waveforms determined by the anatomic position of the vessel as well as cardiac- and respiration-related pressure variations. These waveforms are also affected by various physiologic and pathologic conditions. Resistive index (systolic velocity – diastolic velocity/systolic velocity), the arterial pulsatility index (systolic velocity – diastolic velocity/mean velocity), and the venous pulsatility index (systolic velocity/diastolic velocity) are examples of quantitative biomarkers developed for describing changes in vascular flow. These biomarkers can be used in hepatic artery, hepatic vein, and portal vein imaging. For NAFLD or NASH diagnosis, predominantly portal vein–based indexes have been investigated and therefore are the focus of this section (46). Hepatic vein– and artery–based indexes are outside of the scope of this review; however, these methods, and newer methods like subharmonic imaging, can be used in evaluation of advanced CLD (47,48).

Portal venous pulsatility index, calculated as (maximum velocity – minimum velocity)/maximum velocity (Fig 8), may be useful for the diagnosis of NASH with significant fibrosis. In a recent study of 123 patients, pulsatility index was shown to have a high AUC (0.84 [95% CI: 0.77, 0.91]) in the detection of biopsy-proven high-risk fatty liver (46). The low cost and excellent availability of hepatic Doppler US and the magnitude of information that can be extracted by means of waveform analysis suggest that this will remain an area of active research for improving the diagnosis and staging of liver pathology. New machine learning techniques will likely find a role in automated calculation of Doppler waveform–based biomarkers as well as finding new biomarkers that may be difficult to discern with visual inspection of spectral waveforms. The focus of these automated techniques will likely be to automate vessel identification, subsequent Doppler activation, and measurement of the quantitative parameters of interest.

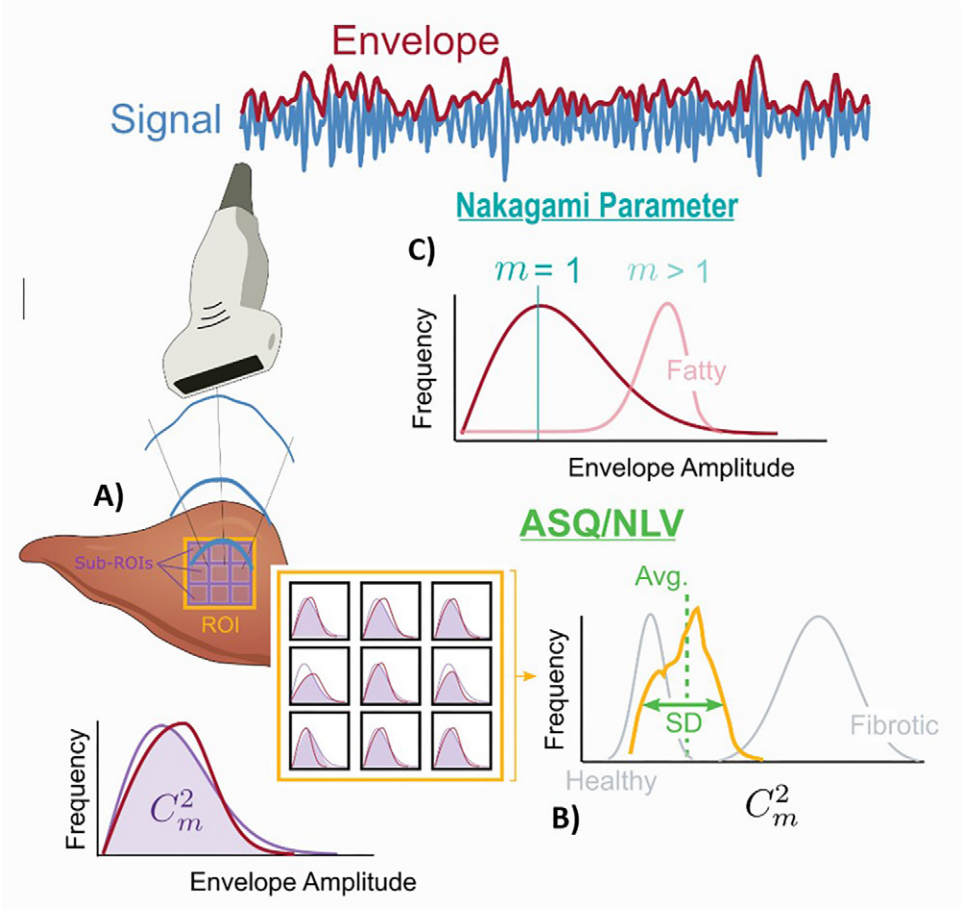

Figure 6: Diagram shows liver fat quantification with the acoustic structure quantification (ASQ), normalized local variance (NLV), and Nakagami parameter methods. **(A)** ASQ and NLV are calculated by comparing the theoretical and real envelope distributions of backscattered US signal (purple and red distribution curves). The magnitude of the fitting between these two curves is calculated as the Cm^2 value. This value is calculated in multiple small regions of interest (ROIs). **(B)** The distribution of these multiple Cm^2 values is plotted. The ASQ method uses the differences between these plots to differentiate fibrotic tissue. NLV is calculated according to similar principles; however, it is mainly used for steatosis quantification. **(C)** The Nakagami parameter is the variation in the shape of the envelope distribution of backscattered US signal (red distribution on the blue curve). This variation is estimated as the *m* value, which is also called *shape parameter*. Higher *m* values are observed in fatty liver tissues.

Multiparametric Models

Multiparametric models using US-derived imaging markers have recently been developed to identify patients with high-risk NASH. The FibroScan–aspartate aminotransferase score combines FibroScan (Echosens) measurements of liver stiffness and the controlled attenuation parameter with aspartate aminotransferase levels. This score has been reported to have good diagnostic performance in the detection of NASH (identified as NAFLD activity score ≥5), with an AUC of 0.75 (95% CI: 0.69, 0.81) and slightly superior results to liver stiffness measurement alone; however, the AUC (0.68 [95% CI: 0.61, 0.75]) to detect F2 grade or higher was lower than that for liver stiffness measurement alone (0.82 [95% CI: 0.76, 0.87]) (49). Another combination model, LAD-NASH score, has been developed by combining three US features: liver stiffness, AC, and dispersion slope. Performance of this score in the detection of patients with high-risk NASH was good in two study samples from different countries (Japan, 111 patients with NAFLD [AUC, 0.86 {95% CI: 0.79, 0.93}]; Korea, 102 patients with NAFLD [AUC, 0.88 {95% CI: 0.80, 0.95}]) (4).

Despite encouraging early results, US-derived multiparametric models have several limitations. One major disadvantage is the existence of a large "gray zone." Both the FibroScan–aspartate aminotransferase and LAD-NASH scores use a dual cutoff approach where low and high cutoff values are used to rule out and rule in high-risk NASH. The gray zone, where results are too indeterminate to support clinical decision-making, lies between these. In the training cohorts of the FibroScan–aspartate aminotransferase and LAD-NASH scores, 39% and 26% of patients fell into this category, respectively. To narrow the gray zone, sequential testing using different noninvasive tests and other imaging modalities has been proposed, with liver biopsy as a last resort (4,50).

Multiparametric US–based model components may not be readily available, create extra cost and time burdens for health care providers and patients, and be clinically unreliable in specific circumstances. For example, the FibroScan–aspartate aminotransferase score relies on aspartate aminotransferase levels, which may show poor correlation with disease severity (51). In the case of the LAD-NASH score, dispersion slope measurement is required. This parameter is not yet widely available or routinely obtained.

In summary, for multiparametric US models, quantitative sonographic biomarkers should be evaluated not only in terms of their absolute diagnostic value, but also their incremental value relative to other readily available sonographic biomarkers. These models may be used as enrichment biomarkers to select patients with high-risk NASH for future clinical trials. More studies are needed to understand the role of these models.

Artificial Intelligence

AI applications in liver US imaging are growing quickly, with many innovative approaches reported in the literature (52). For example, Byra et al (53) recently developed image analysis algorithms to detect PDFF-defined steatosis on multiview US images. Multiview algorithms could diagnose greater than 5% steatosis with an AUC of 0.91 and greater than 10% steatosis with an AUC of 0.86. Combining US images from multiple

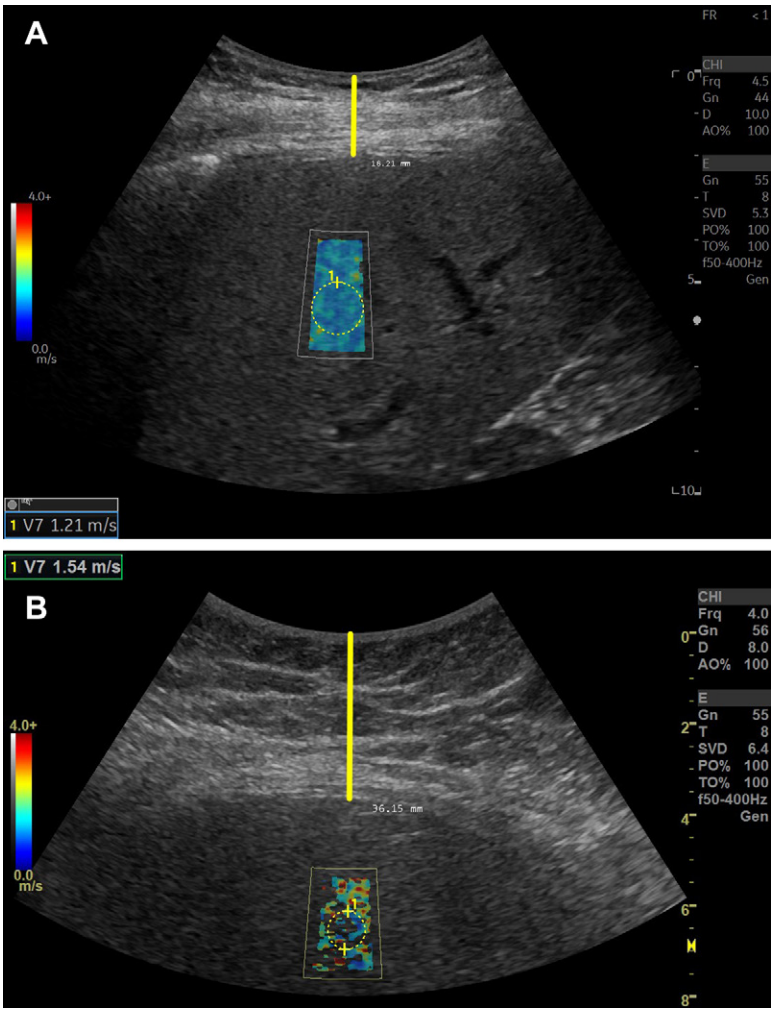

Figure 7: Shear-wave elastography (SWE) signal quality may be affected by the thickness of the subcutaneous tissue or skin-to–liver capsule distance. **(A)** SWE image in a 74-year-old female patient with clinically suspected nonalcoholic fatty liver disease (NAFLD). SWE examination was performed, and a complete SWE value pixel map was observed. The shear-wave speed, or SWS, color spectrum is presented on the left side (red, high SWS; dark blue, low SWS). Skin-to–liver capsule distance was estimated as 1.8 cm (vertical yellow line). The SWS value is presented in the bottom left corner of the image. SWS values are generated from the circular region of interest. **(B)** SWE image in a 35-year-old female patient with clinically suspected NAFLD. SWE examination was performed, and poor SWE value pixel map fill-in was observed. Skin-to–liver capsule distance was estimated as 3.6 cm (vertical yellow line). The SWS value is presented in the top left corner of the image. SWS values are generated from the circular region of interest.

views with the help of deep learning may be valuable, as it would provide a whole-organ assessment of the liver tissue.

AI methods for radiofrequency signal processing have also been studied. For example, Han et al (54) used a deep learning approach to classify US radiofrequency data to quantify steatosis by accepting MRI PDFF values as the reference standard. The authors reported a strong linear relationship between the deep learning–predicted fat fraction and MRI PDFF results (Pearson $r = 0.85$). Jeon et al (55) used two-dimensional neural networks to study B-mode images and tissue scatter distribution imaging and tissue attenuation imaging data in a PDFF-defined sample of patients with NAFLD. The algorithm output could identify greater than 5% steatosis with an AUC of 0.97 (95% CI: 0.93, 0.99), which was higher than tissue attenuation imaging, tissue scatter distribution imaging, and B-mode–based visual decision ($P = .01$, $P = .006$, and $P < .001$, respectively). These results show that analyzing radiofrequency data with the help of deep learning may provide superior performance in the diagnosis of steatosis compared with existing conventional methods.

AI in US is rapidly evolving, with multiple FDA-cleared models commercially available, particularly for cardiac applications. Despite emerging literature, FDA-cleared NAFLD-focused AI-enabled devices are not yet widely available (56). Currently, most of the published US NAFLD management algorithms focus on diagnostic accuracy. However, early disease detection, reprioritization of cases for radiologist review, and personalized diagnostics by comparing prior examinations are alternative approaches that may improve NAFLD management (57,58). To give specific examples, early AI-enhanced steatosis quantification may be helpful for making lifestyle changes earlier in life. Identifying patients at risk for developing advanced CLD, like those with high-risk NASH, from US images and reprioritizing these images for more detailed review could facilitate better detection. Comparing prior US images and analyzing the differences in liver tissue characteristics may ultimately be important for monitoring treatment response.

Consensus Efforts

Several expert societies and committees have convened groups to develop guidelines and consensus recommendations based on multicenter phantom and clinical studies. These activities are necessary, as complex multiparametric quantitative imaging methods require standardization to minimize variability. The Society of Radiologists in Ultrasound and the RSNA Quantitative Imaging Biomarkers Alliance, or QIBA, Ultrasound Shear Wave Speed Committees developed separate but complementary recommendations for SWE practice that aim to aid interpretation and decrease variability (37,59).

The American Institute of Ultrasound in Medicine/RSNA QIBA Pulse-Echo Quantitative US group has been working to develop consensus guidelines and profiles for attenuation, backscatter coefficient, and SoS methods (7).

Conclusion

Since the late 1960s, scientists have studied hepatic fat accumulation with conventional sonographic imaging techniques (60,61). In the intervening years, advances in US hardware, signal processing, computational efficiency, and analytic algorithm development have led to new, exciting, and powerful quantitative imaging tools that promise to increase hepatic steatosis diagnostic accuracy and reliability.

Early nonalcoholic fatty liver disease (NAFLD) diagnosis and timely clinical management are the main motivating factors for developing noninvasive biomarkers. The low cost, wide

availability, and lack of harm of diagnostic US combined with the prevalence and public health importance of NAFLD suggest that US-based techniques will continue to be used for the foreseeable future. Limited evidence, device and operator variability, and patient-related factors like obesity are common limitations for some US biomarkers. Innovative research that combines multiparametric sonographic parameters with advanced machine learning and acoustic signal processing techniques are likely to further improve the clinical utility of diagnostic US in NAFLD care. Advanced sonographic techniques are likely to grow further and become an integral part of NAFLD care for diagnosis, risk stratification, and response to therapy assessment in the next few years.

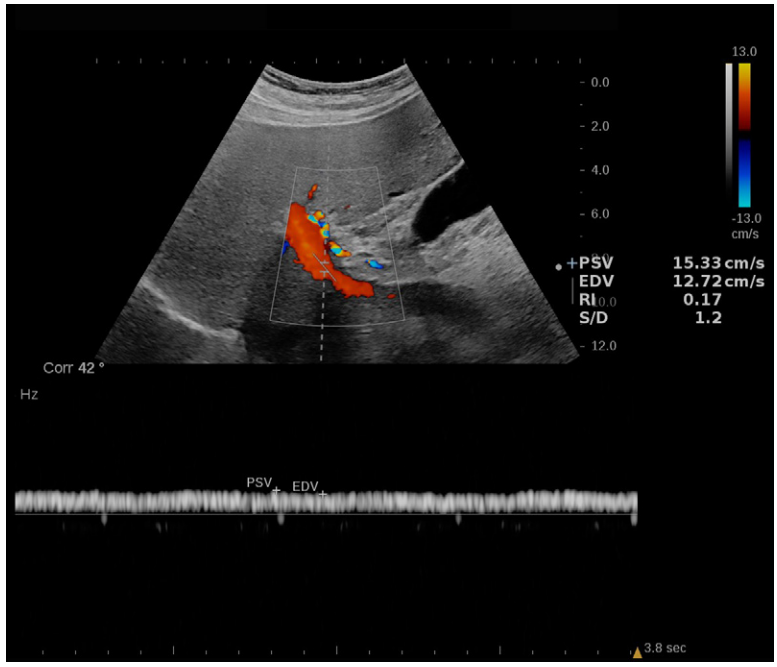

Figure 8: Doppler US image in a 72-year-old male patient with nonalcoholic steatohepatitis (NASH) and grade 1 steatosis. An example of a portal vein spectral Doppler image with flow speed maximum of 15.33 cm/sec and minimum of 12.72 cm/sec. The colored scale bar on the left represents the flow speed spectrum based on the flow direction. The graph on the bottom represents the Doppler spectrum and its association with flow velocity. Increased portal vein pulsatility index [(maximum velocity – minimum velocity)/maximum velocity] may be associated with NASH (46). Reproduced, with permission, from the Non-Invasive Biomarkers of Metabolic Liver Disease, or NIMBLE 1.1, study (18).

Disclosures of conflicts of interest: A.O. Member of the editorial advisory board for *Ultrasound in Medicine and Biology* and editor of *WFUMB Ultrasound Open*; committee member for the American Institute of Ultrasound in Medicine (AIUM), the RSNA Quantitative Imaging Biomarkers Alliance (QIBA), and Society of Abdominal Radiology (SAR); AIUM QIBA PEQUS Attenuation group co-chair; patents pending for AI liver imaging; payment for consultant services from AutonomUS Medical Technologies. **V.K.** Patents or patents pending with Massachusetts General Hospital and GE HealthCare. **T.T.P.** Grants to institution from GE and SAR; honoraria from the Massachusetts Society of Radiologic Technologists and Zhejiang Medical Association; clinical trial reviewer for Non-Invasive Biomarkers of Metabolic Liver Disease (NIMBLE); chair of the Artificial Intelligence and Machine Learning Working Group, Advanced Ultrasound Techniques Emerging Technology Commission, SAR and of the Sound Speed Workgroup, AIUM/RSNA QIBA Pulse-echo Quantitative Ultrasound Biomarker Committee. **Q.L.** No relevant relationships. **M.B.** No relevant relationships. **I.R.M.** Consulting fees from Siemens Healthineers; honorarium from the American Association of Physicists in Medicine (AAPM); travel support from the AAPM; U.S. patent for ultrasonic imaging system with angularly compounded acoustic radiation force excitation; co-chair of the RSNA QIBA Pulse Echo Quantitative Ultrasound Biomarker Committee; system loan and technical support from Siemens Healthineers and GE HealthCare. **M.W.** Co-chair of the AIUM/QIBA Pulse-echo Quantitative Ultrasound Committee. **P.G.** No relevant relationships. **S.S.** Patents or patents pending with Harvard Medical School and Massachusetts General Hospital. **Y.G.** No relevant relationships. **S.D.** No relevant relationships. **J.R.G.** Royalties from Elsevier. **A.E.S.** Royalties or licenses with Katharos Labs and AutonomUS Medical Technologies; consulting fees from AstraZeneca, Bracco Diagnostics, Bristol Myers Squibb, GE, Gerson Lehrman Group, Guidepoint Global Advisors, Supersonic Imagine, Novartis, Pfizer, Philips, Parexel Informatics, and WorldCare Clinical; payment for expert testimony from Matis Baum and O'Connor; patents or patents pending for US laser guidance device, US apparatus, sonographer fatigue monitoring, optical biopsy needle and endoscope system, optical pathology systems and methods, noncontact laser US system, personalized fit face mask, system and methods for portable US-guided cannulation, and systems and methods for analyte detection using electromagnetically induced resonance; advisory or scientific board member for Analogic, U.S. Department of Defense, Fujifilm Healthcare, Foundation for the National Institutes of Health, GE, National Institutes of Health, and Philips; leadership or fiduciary role for AIUM and AutonomUS Medical Technologies; stock or stock options in Avira, AutonomUS Medical Technologies, Evidence Based Psychology, Klea, Katharos Labs, Quantix Bio, Sonoluminous, Rhino Health, and Ochre Bio; equipment, materials, or gifts from Analogic, Canon, Echosens, GE, Hitachi, Philips, Siemens, Supersonic Imagine/Hologic, and Toshiba Medical Systems.

References

1. Moon AM, Singal AG, Tapper EB. Contemporary epidemiology of chronic liver disease and cirrhosis. Clin Gastroenterol Hepatol 2020;18(12):2650–2666.
2. Benedict M, Zhang X. Non-alcoholic fatty liver disease: an expanded review. World J Hepatol 2017;9(16):715–732.
3. Vilar-Gomez E, Vuppalanchi R, Mladenovic A, et al. Prevalence of high-risk nonalcoholic steatohepatitis (NASH) in the United States: results from NHANES 2017-2018. Clin Gastroenterol Hepatol 2023;21(1):115–124.e7.
4. Sugimoto K, Lee DH, Lee JY, et al. Multiparametric US for identifying patients with high-risk NASH: a derivation and validation study. Radiology 2021;301(3):625–634.
5. Ajmera V, Park CC, Caussy C, et al. Magnetic resonance imaging proton density fat fraction associates with progression of fibrosis in patients with nonalcoholic fatty liver disease. Gastroenterology 2018;155(2):307–310.e2.
6. Moura Cunha G, Navin PJ, Fowler KJ, Venkatesh SK, Ehman RL, Sirlin CB. Quantitative magnetic resonance imaging for chronic liver disease. Br J Radiol 2021;94(1121):20201377.
7. Fetzer DT, Rosado-Mendez IM, Wang M, et al. Pulse-echo quantitative US biomarkers for liver steatosis: toward technical standardization. Radiology 2022;305(2):265–276.
8. Wu S, Tu R, Zheng E, Shi Y, Liu G. Findings and implications of focal fatty sparing of the liver at follow-up: a preliminary study based on sonography, computed tomography, and magnetic resonance imaging. J Ultrasound Med 2013;32(10):1695–1702.
9. Hernaez R, Lazo M, Bonekamp S, et al. Diagnostic accuracy and reliability of ultrasonography for the detection of fatty liver: a meta-analysis. Hepatology 2011;54(3):1082–1090.
10. Hirooka M, Koizumi Y, Sunago K, et al. Efficacy of B-mode ultrasound-based attenuation for the diagnosis of hepatic steatosis: a systematic review/meta-analysis. J Med Ultrason 2022;49(2):199–210.
11. Ferraioli G, Soares Monteiro LB. Ultrasound-based techniques for the diagnosis of liver steatosis. World J Gastroenterol 2019;25(40):6053–6062.
12. Ferraioli G, Berzigotti A, Barr RG, et al. Quantification of liver fat content with ultrasound: a WFUMB position paper. Ultrasound Med Biol 2021;47(10):2803–2820.
13. Moret A, Boursier J, Houssel Debry P, et al. Evaluation of the hepatorenal B-mode ratio and the "controlled attenuation parameter" for the detection and grading of steatosis. Ultraschall Med 2022;43(5):479–487.
14. Stahlschmidt FL, Tafarel JR, Menini-Stahlschmidt CM, Baena CP. Hepatorenal index for grading liver steatosis with concomitant fibrosis. PLoS One 2021;16(2):e0246837.
15. Cha DI, Kang TW, Min JH, et al. Deep learning-based automated quantification of the hepatorenal index for evaluation of fatty liver by ultrasonography. Ultrasonography 2021;40(4):565–574.

16. Ferraioli G, Kumar V, Ozturk A, Nam K, de Korte CL, Barr RG. US attenuation for liver fat quantification: an AIUM-RSNA QIBA Pulse-Echo Quantitative Ultrasound initiative. Radiology 2022;302(3):495–506.
17. Jang JK, Choi SH, Lee JS, Kim SY, Lee SS, Kim KW. Accuracy of the ultrasound attenuation coefficient for the evaluation of hepatic steatosis: a systematic review and meta-analysis of prospective studies. Ultrasonography 2022;41(1):83–92.
18. Sanyal AJ, Shankar SS, Calle RA, et al. Non-invasive biomarkers of nonalcoholic steatohepatitis: the FNIH NIMBLE project. Nat Med 2022;28(3):430–432.
19. Alshagathrh FM, Househ MS. Artificial intelligence for detecting and quantifying fatty liver in ultrasound images: a systematic review. Bioengineering (Basel) 2022;9(12):748.
20. Lin SC, Heba E, Wolfson T, et al. Noninvasive diagnosis of nonalcoholic fatty liver disease and quantification of liver fat using a new quantitative ultrasound technique. Clin Gastroenterol Hepatol 2015;13(7):1337–1345.e6.
21. Han A, Zhang YN, Boehringer AS, et al. Assessment of hepatic steatosis in nonalcoholic fatty liver disease by using quantitative US. Radiology 2020;295(1):106–113.
22. Labyed Y, Milkowski A. Novel method for ultrasound-derived fat fraction using an integrated phantom. J Ultrasound Med 2020;39(12):2427–2438.
23. Wear KA, Han A, Rubin JM, et al. US backscatter for liver fat quantification: an AIUM-RSNA QIBA Pulse-Echo Quantitative Ultrasound initiative. Radiology 2022;305(3):526–537.
24. Popa A, Bende F, Şirli R, et al. Quantification of liver fibrosis, steatosis, and viscosity using multiparametric ultrasound in patients with non-alcoholic liver disease: a "real-life" cohort study. Diagnostics (Basel) 2021;11(5):783.
25. Dillman JR, Thapaliya S, Tkach JA, Trout AT. Quantification of hepatic steatosis by ultrasound: prospective comparison with MRI proton density fat fraction as reference standard. AJR Am J Roentgenol 2022;219(5):784–791.
26. Gao J, Wong C, Maar M, Park D. Reliability of performing ultrasound derived SWE and fat fraction in adult livers. Clin Imaging 2021;80:424–429.
27. Son J, Lee JY, Yi NJ, et al. Hepatic steatosis: assessment with acoustic structure quantification of US imaging. Radiology 2016;278(1):257–264.
28. Lee DH, Lee JY, Park MS, Han JK. Non-invasive monitoring of hepatic steatosis via acoustic structure quantification of ultrasonography with MR spectroscopy as the reference standard. Ultrasonography 2020;39(1):70–78.
29. Lin YH, Wan YL, Tai DI, et al. Considerations of ultrasound scanning approaches in non-alcoholic fatty liver disease assessment through acoustic structure quantification. Ultrasound Med Biol 2019;45(8):1955–1969.
30. Bae JS, Lee JY, Lee DH, Kim H, Lee Y, Han JK. Quantitative evaluation of hepatic steatosis using normalized local variance in a rat model: comparison with histopathology as the reference standard. Korean J Radiol 2019;20(9):1399–1407.
31. Zhao Y, Zhang C, Xu S, et al. Quantitative evaluation of hepatic steatosis using novel ultrasound technology normalized local variance (NLV) and its standard deviation with different ROIs in patients with metabolic-associated fatty liver disease: a pilot study. Abdom Radiol (NY) 2022;47(2):693–703.
32. Gao J, Lee R, Trujillo M. Reliability of performing multiparametric ultrasound in adult livers. J Ultrasound Med 2022;41(3):699–711.
33. Pirmoazen AM, Khurana A, Loening AM, et al. Diagnostic performance of 9 quantitative ultrasound parameters for detection and classification of hepatic steatosis in nonalcoholic fatty liver disease. Invest Radiol 2022;57(1):23–32.
34. Kaliaev A, Chavez W, Soto J, et al. Quantitative ultrasound assessment of hepatic steatosis. J Clin Exp Hepatol 2022;12(4):1091–1101.
35. Park J, Lee JM, Lee G, Jeon SK, Joo I. Quantitative evaluation of hepatic steatosis using advanced imaging techniques: focusing on new quantitative ultrasound techniques. Korean J Radiol 2022;23(1):13–29.
36. Ozturk A, Grajo JR, Dhyani M, Anthony BW, Samir AE. Principles of ultrasound elastography. Abdom Radiol (NY) 2018;43(4):773–785.
37. Barr RG, Wilson SR, Rubens D, Garcia-Tsao G, Ferraioli G. Update to the Society of Radiologists in Ultrasound Liver Elastography Consensus Statement. Radiology 2020;296(2):263–274.
38. Bruce M, Kolokythas O, Ferraioli G, Filice C, O'Donnell M. Limitations and artifacts in shear-wave elastography of the liver. Biomed Eng Lett 2017;7(2):81–89.
39. Sugimoto K, Moriyasu F, Oshiro H, et al. Clinical utilization of shear wave dispersion imaging in diffuse liver disease. Ultrasonography 2020; 39(1):3–10.
40. Lee DH, Cho EJ, Bae JS, et al. Accuracy of two-dimensional shear wave elastography and attenuation imaging for evaluation of patients with nonalcoholic steatohepatitis. Clin Gastroenterol Hepatol 2021;19(4):797–805.e7.
41. Jang JK, Lee ES, Seo JW, et al. Two-dimensional shear-wave elastography and US attenuation imaging for nonalcoholic steatohepatitis diagnosis: a cross-sectional, multicenter study. Radiology 2022;305(1):118–126.
42. D'Hondt A, Rubesova E, Xie H, Shamdasani V, Barth RA. Liver fat quantification by ultrasound in children: a prospective study. AJR Am J Roentgenol 2021;217(4):996–1006.
43. Deffieux T, Gennisson JL, Bousquet L, et al. Investigating liver stiffness and viscosity for fibrosis, steatosis and activity staging using shear wave elastography. J Hepatol 2015;62(2):317–324.
44. Deng Y, Palmeri ML, Rouze NC, Haystead CM, Nightingale KR. Evaluating the benefit of elevated acoustic output in harmonic motion estimation in ultrasonic shear wave elasticity imaging. Ultrasound Med Biol 2018;44(2):303–310.
45. Ormachea J, Parker KJ, Barr RG. An initial study of complete 2D shear wave dispersion images using a reverberant shear wave field. Phys Med Biol 2019;64(14):145009.
46. Baikpour M, Ozturk A, Dhyani M, et al. Portal venous pulsatility index: a novel biomarker for diagnosis of high-risk nonalcoholic fatty liver disease. AJR Am J Roentgenol 2020;214(4):786–791.
47. Gupta I, Eisenbrey JR, Machado P, et al. Diagnosing portal hypertension with noninvasive subharmonic pressure estimates from a US contrast agent. Radiology 2021;298(1):104–111.
48. Barr RG, Ferraioli G. Multiparametric Ultrasound for the Assessment of Diffuse Liver Disease: A Practical Approach. Elsevier; 2023.
49. Lee JS, Lee HW, Kim BK, et al. Comparison of FibroScan-aspartate aminotransferase (FAST) score and other non-invasive surrogates in predicting high-risk non-alcoholic steatohepatitis criteria. Front Med (Lausanne) 2022;9:869190.
50. Noureddin N, Alkhouri N, Brown KA, Noureddin M. Driving nonalcoholic steatohepatitis forward using the FibroScan aspartate aminotransferase score, but obey the traffic lights. Hepatology 2020;72(6):2228–2230.
51. Ahmed Z, Ahmed U, Walayat S, et al. Liver function tests in identifying patients with liver disease. Clin Exp Gastroenterol 2018;11:301–307.
52. Cao L-L, Peng M, Xie X, et al. Artificial intelligence in liver ultrasound. World J Gastroenterol 2022;28(27):3398–3409.
53. Byra M, Han A, Boehringer AS, et al. Liver fat assessment in multiview sonography using transfer learning with convolutional neural networks. J Ultrasound Med 2022;41(1):175–184.
54. Han A, Byra M, Heba E, et al. Noninvasive diagnosis of nonalcoholic fatty liver disease and quantification of liver fat with radiofrequency ultrasound data using one-dimensional convolutional neural networks. Radiology 2020;295(2):342–350.
55. Jeon SK, Lee JM, Joo I, Yoon JH, Lee G. Two-dimensional convolutional neural network using quantitative US for noninvasive assessment of hepatic steatosis in NAFLD. Radiology 2023;307(1):e221510.
56. Artificial Intelligence/Machine Learning (AI/ML)-Based Software as a Medical Device (SaMD) Action Plan. U.S. Food and Drug Administration. https://www.fda.gov/media/145022/download. Published January 2021. Accessed September 22, 2021.
57. Acosta JN, Falcone GJ, Rajpurkar P. The need for medical artificial intelligence that incorporates prior images. Radiology 2022;304(2):283–288.
58. van Leeuwen KG, de Rooij M, Schalekamp S, van Ginneken B, Rutten MJCM. How does artificial intelligence in radiology improve efficiency and health outcomes? Pediatr Radiol 2022;52(11):2087–2093.
59. Chen S, Dhyani M, Garra B, Hall T, Palmeri M. QIBA Ultrasound Shear Wave Speed Biomarker update. Ultrasound Med Biol 2017;43:S149.
60. Wells PN, McCarthy CF, Ross FG, Read AE. Comparison of A-scan and compound B-scan ultrasonography in the diagnosis of liver disease. Br J Radiol 1969;42(503):818–823.
61. Behan M, Kazam E. The echographic characteristics of fatty tissues and tumors. Radiology 1978;129(1):143–151.
62. Ferraioli G, Filice C, Castera L, et al. WFUMB guidelines and recommendations for clinical use of ultrasound elastography: part 3: liver. Ultrasound Med Biol 2015;41(5):1161–1179.
63. Shiina T, Nightingale KR, Palmeri ML, et al. WFUMB guidelines and recommendations for clinical use of ultrasound elastography: part 1: basic principles and terminology. Ultrasound Med Biol 2015;41(5):1126–1147.
64. Ferraioli G. Review of liver elastography guidelines. J Ultrasound Med 2019;38(1):9–14.
65. Johnson SI, Fort D, Shortt KJ, et al. Ultrasound stratification of hepatic steatosis using hepatorenal index. Diagnostics (Basel) 2021;11(8):1443.
66. Cloutier G, Destrempes F, Yu F, Tang A. Quantitative ultrasound imaging of soft biological tissues: a primer for radiologists and medical physicists. Insights Imaging 2021;12(1):127.
67. Ormachea J, Parker KJ. A preliminary study of liver fat quantification using reported ultrasound speed of sound and attenuation parameters. Ultrasound Med Biol 2022;48(4):675–684.

68. Tsai Y-W, Zhou Z, Gong CA, et al. Ultrasound detection of liver fibrosis in individuals with hepatic steatosis using the Homodyned K distribution. Ultrasound Med Biol 2021;47(1):84–94.
69. Bae JS, Lee DH, Lee JY, et al. Quantitative assessment of fatty liver using ultrasound with normalized local variance technique. Ultraschall Med 2021;42(6):599–606.
70. Chuang Y-H, Hsieh C-S, Lai M-W, et al. Detection of pediatric hepatic steatosis through ultrasound backscattering analysis. Eur Radiol 2021;31(5):3216–3225.
71. Zhou Z, Wu W, Wu S, Jia K, Tsui P-H. A review of ultrasound tissue characterization with mean scatterer spacing. Ultrason Imaging 2017;39(5):263–282.
72. Insana MF, Wagner RF, Garra BS, Brown DG, Shawker TH. Analysis of ultrasound image texture via generalized rician statistics. Proc SPIE 1985;0665:153–159.
73. Rubert N, Varghese T. Mean scatterer spacing estimation using multitaper coherence. IEEE Trans Ultrason Ferroelectr Freq Control 2013;60(6):1061–1073.
74. Varghese T, Donohue KD. Mean-scatterer spacing estimates with spectral correlation. J Acoust Soc Am 1994;96(6):3504–3515.
75. Molthen RC, Narayanan VM, Shankar PM, et al. Using phase information in ultrasonic backscatter for in vivo liver analysis. Ultrasound Med Biol 1998;24(1):79–91.
76. Basavarajappa L, Baek J, Reddy S, et al. Multiparametric ultrasound imaging for the assessment of normal versus steatotic livers. Sci Rep 2021;11(1):2655.
77. Parker KJ. Scattering and reflection identification in H-scan images. Phys Med Biol 2016;61(12):L20–L28.